Journal of Biomechanics 188 (2025) 112784

Contents lists available at ScienceDirect

Journal of Biomechanics

journal homepage: www.elsevier.com/locate/jbiomech

Effects of an elastic hip exoskeleton on stability quantified by mechanical energetics and whole-body angular momentum during walking with treadmill belt speed perturbations

Pawel R. Golyski [a,b,*], Nicholas K. Swaich [b], Fausto A. Panizzolo [c], Gregory S. Sawicki [a,b,d,e]

[a] Parker H. Petit Institute for Bioengineering and Biosciences, Georgia Institute of Technology, Atlanta, GA, USA
[b] George W. Woodruff School of Mechanical Engineering, Georgia Institute of Technology, Atlanta, GA, USA
[c] Moveo s.r.l., Padova, PD, Italy
[d] Institute for Robotics and Intelligent Machines, Georgia Institute of Technology, Atlanta, GA, USA
[e] School of Biological Sciences, Georgia Institute of Technology, Atlanta, GA, USA

ARTICLE INFO

Keywords:
Angular Momentum
Mechanical Energy
Exoskeletons
Balance
Slips

ABSTRACT

Relative to motorized devices, passive hip exoskeletons with elastic actuation provide cheaper and lower-profile solutions to assist locomotion during walking. However, the influence of elastic hip assistance on stability during walking is poorly understood. Here, we investigated the effects on stability of a hip exoskeleton that provided elastic flexion torque during late stance. We quantified stability using both sagittal whole-body angular momentum (WBAM) range and whole-body mechanical work during walking with unexpected anteroposterior treadmill belt accelerations among 11 healthy uninjured individuals. We hypothesized that during perturbations, 1) an elastic hip exoskeleton would improve stability as measured by a smaller range in sagittal WBAM and a lower whole-body energetic demand imposed by the perturbation, and 2) this improvement in whole-body energetic demand would be mediated by the exoskeleton shifting the local mechanical energetics of the hip joint to oppose the energetic demands of the perturbation. Contrary to our hypotheses, the elastic hip exoskeleton did not influence whole-body work demands imposed by perturbations ($p>0.226$). Additionally, while sagittal WBAM ranges were larger during unperturbed walking with increasing exoskeleton stiffness due to alterations in trunk kinematics ($p<0.001$), this effect did not extend to perturbed walking ($p>0.419$). Further, while higher exoskeleton stiffnesses (0.66–1.0 Nm/deg) shifted ipsilateral hip joint work in opposition to whole-body work demands, the same stiffnesses shifted contralateral hip joint work toward whole-body work demands. Our findings demonstrate conclusions drawn about stability from sagittal WBAM range do not carry over from unperturbed to perturbed walking.

1. Introduction

Lower-limb exoskeletons have been designed for a wide variety of applications, including lowering the metabolic cost of locomotion (Nasiri et al., 2018; Panizzolo et al., 2019; Sawicki et al., 2020; Shepertycky et al., 2021; Witte et al., 2020), reducing risk of injury (Lamers and Zelik, 2021; Li et al., 2021), offloading limbs during continuous industrial tasks (Dooley et al., 2023), facilitating rehabilitation (Banala et al., 2009; Patton et al., 2008), and improving locomotor stability. We define locomotor stability as the ability to respond to large external mechanical perturbations such that an individual experiences minimal deviation from steady state (i.e., unperturbed) locomotion while also being able to rapidly return to steady state locomotion following the perturbation. Exoskeletal approaches providing stabilizing assistance as needed (i.e., approaches that augment, but do not replace lower limb function) have been limited to either providing powered hip flexion and extension torques to increase anteroposterior margin of stability following treadmill accelerations during walking (Monaco et al., 2017) and providing powered hip abduction and adduction torques to maintaining mediolateral margin of stability following unexpected pushes during walking (Zhang et al., 2018). Devices actuated by elastic elements, most often targeting the ankle or hip joints, provide an attractive alternative to active, motor-driven devices since they can be cheaper, lighter, and do not require tuning of sophisticated hardware, while also

* Corresponding author at: Parker H. Petit Institute for Bioengineering and Biosciences, Georgia Institute of Technology, Atlanta, GA, USA.
E-mail address: pgolyski3@gatech.edu (P.R. Golyski).

https://doi.org/10.1016/j.jbiomech.2025.112784
Accepted 26 May 2025
Available online 27 May 2025

being able to augment selected locomotor objectives, most often the improvement of walking and running economy (Collins et al., 2015; Nasiri et al., 2018; Panizzolo et al., 2019). However, limited prior work has investigated the influence of elastic exoskeletons on stability during walking. To our knowledge, the only study investigating the influence of elastic exoskeletons on locomotion more generally evaluated the influence of elastic ankle exoskeletons during perturbed hopping (Williamson et al., 2023).

From the perspective of mechanical energetics, elastic exoskeletons that provide spring-like assistance in parallel with the hip or ankle may initially seem unlikely to improve stability during walking. To achieve "energetic" stability (i.e., to minimize deviation in mechanical energy from steady state levels during and after a perturbation) during constant speed, level ground walking, over a stride any net mechanical energy injected into the body from the environment must be dissipated, and any net mechanical energy extracted by the environment from the body must be re-generated. This dissipation or re-generation must occur such that the overall energy of the body returns to steady state levels (i.e., net zero work over a stride). Although elastic exoskeletons cannot contribute net mechanical energy, they can temporarily store energy, redistribute energy to other joints, and alter the mechanics of underlying musculature to modulate the biological work at the joints they target (Collins et al., 2015; Farris et al., 2013; Nuckols et al., 2020; Nuckols et al., 2020; Van Dijk and Van Der Kooij, 2014). At the hip joint specifically, previous studies have shown that during walking elastic hip exoskeletons that resist extension and assist flexion can alter distal muscle activations (Haufe et al., 2020) and increase biological hip work (Lewis and Ferris, 2011). However, how such shifts relate to mediating the transient energetic demands of perturbations is unclear.

In this study, we have sought to assess the influence of an elastic hip exoskeleton that resists hip extension and assists flexion on stability through the lens of mechanical energetics during perturbed treadmill walking. Perturbations consisted of transient unilateral anteroposterior belt accelerations delivered in either early or late stance. These perturbations were selected based on previous work demonstrating such perturbations elicit a range of mechanical energetic demands on the lower limbs depending on perturbation timing (Golyski and Sawicki, 2022), and because we anticipated the hip extension elicited by the perturbation would engage the exoskeleton. Additionally, we also sought to quantify stability using a more conventional whole-body mechanical measure of stability – sagittal plane whole-body angular momentum (WBAM) range. Sagittal WBAM captures the kinematic demand of the perturbation – during an anteroposterior belt acceleration or trip, the body is pitched forwards, which results in changes in translational and angular velocities of the body segments relative to the center of mass (COM) (Liu and Finley, 2020; Pijnappels et al., 2004). WBAM and whole-body mechanical work are therefore linked, since whole-body mechanical work also captures segmental angular velocity through segmental rotational kinetic energy. Further, sagittal WBAM normalized to walking speed, body mass, and height or leg length is thought to assess stability since it fluctuates within a narrow range during unperturbed walking in healthy uninjured individuals (~0.027–0.064 at 1.2–1.3 m/s; (Bennett et al., 2010; Herr and Popovic, 2008; Hisano et al., 2023; Silverman and Neptune, 2011)), while this range is broader in populations with balance impairments such as stroke-survivors (~0.157 at 0.4 m/s; (Honda et al., 2019)) and individuals with transfemoral amputation (~0.076 at 1.4 m/s; (Hisano et al., 2023)).

To understand the influence of elastic hip extension resistance and flexion assistance during perturbed walking on stability in the anteroposterior direction as quantified using WBAM and mechanical energetics, we tested two hypotheses. First, H1) we hypothesized an elastic hip exoskeleton would decrease sagittal WBAM range and whole-body mechanical work during the perturbed and first recovery strides relative to steady state levels, indicative of improved stability. Second, to evaluate a potential mechanism by which whole-body work would be influenced by the exoskeleton, H2) we hypothesized the exoskeleton would shift the net mechanical work of the hip joints in opposition to the whole body demands of the perturbation (i.e., when the perturbation elicits net positive work at the whole-body level, a shift towards negative work at the hip level would be stabilizing).

2. Methods

2.1. Exoskeleton design

We developed a novel custom elastic hip exoskeleton to assist the hip joint with actuation provided by titanium torsional springs mounted lateral to the hips. This design was selected, in contrast to current designs that use an elastic band over the quadriceps (Chen et al., 2019; Haufe et al., 2020; Panizzolo et al., 2019), to allow for future studies to quantify differences in quadriceps muscle activity and muscle dynamics. The elastic hip exoskeleton (Fig. 1A), which was inspired by that of Chiu et al., 2021, was composed of 3 sections: a torso interface, 2 thigh interfaces, and 2 torsional mechanisms (Fig. 1B). The torsional mechanisms were designed to apply elastic assistance from mid to late stance, similar to the torque–angle relationship of the hip during walking (Shamaei et al., 2013). The torsional mechanisms provided hip extension resistance and hip flexion assistance when the "striker" component of the torsional mechanism, which is coupled to the thigh, collides with the "stopper" component, which is coupled to the pelvis. During this collision, the torsional spring is engaged. The relative thigh to pelvis angle at which the collision occurs (i.e., the "engagement angle") can be modified using two steel pins. Each mechanism had 4 stiffness configurations: a no spring configuration (K0), in addition to 0.33 Nm/deg (K1), 0.66 Nm/deg (K2), and 1 Nm/deg (K3) configurations. A range of stiffnesses was selected since we did not anticipate results would monotonically increase with stiffness – literature has demonstrated elastic exoskeleton users adapt their kinematics in response to stiffness, which can result in a stiffness that optimizes performance (Collins et al., 2015). The specific range was selected based on approximating assistive hip flexion stiffness of prior exoskeletons (0.17–1.5 Nm/deg; (Chen et al., 2019; Haufe et al., 2020; Lenzi et al., 2013; Nasiri et al., 2018; Panizzolo et al., 2019; Young et al., 2017)). Additional information about the hip exoskeleton design is included as **Supplementary Material**.

2.2. Experimental protocol

11 healthy, uninjured individuals (10 males, 1 female, mean [SD] age: 23 [3] years, stature: 182.1 [6.6] cm, body mass: 77.2 [11.3] kg) participated in this study after providing informed consent to the protocol approved by the local Institutional Review Board. Each participant underwent a training session and a testing session 2–8 days later. The training session consisted of 20 min of unperturbed walking at 1.25 m/s in each stiffness condition. Additional details about the training protocol are included as **Supplementary Material**. During the testing session, each participant was fitted with the exoskeleton in the K0 condition and walked unperturbed for 2 min at 1.25 m/s on an instrumented split-belt treadmill (CAREN, Motek, Netherlands). The midrange (mean of maximum and minimum) mechanism angle from the last 20 s of this K0 condition was selected as the engagement angle of each participant. The midrange angle was chosen since it approximately coincides with midstance (Shamaei et al., 2013). Engagement angles for all participants were set to begin torque at 20 degrees of mechanism flexion, except for one participant where the mechanisms were set at 10 degrees flexion. Following engagement angle determination, each participant completed 4 blocks of testing, each in a different spring configuration (K0-K3), with the order of configurations being pseudo-randomized. Within each block, each participant first walked unperturbed for 2 min at 1.25 m/s, then walked for approximately 15 min while experiencing transient, unilateral anteroposterior belt accelerations (i.e., belt speed increased from 1.25 to 2.5 m/s and decreased from 2.5 m/s to 1.25 m/s at 15 m/s^2

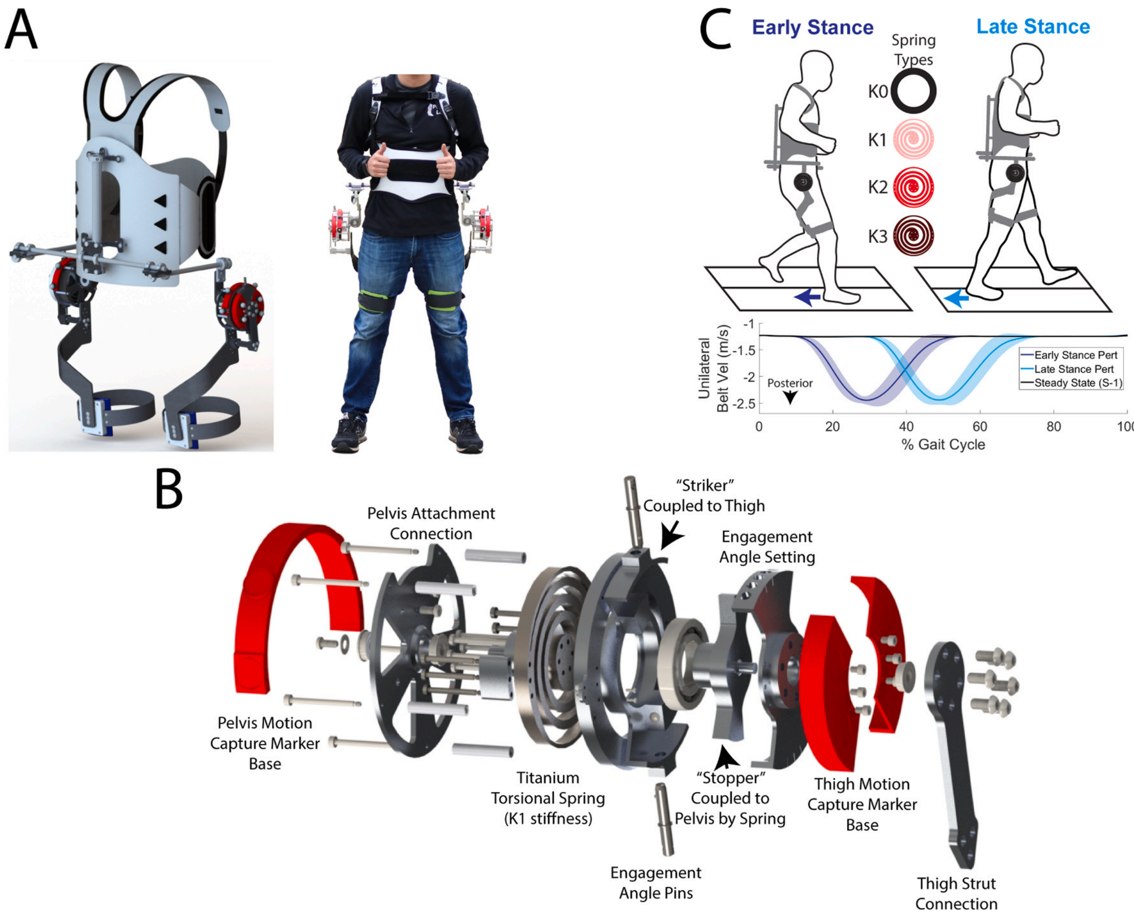

Fig. 1. (A) Torsional elastic hip exoskeleton rendering (left) and the physical device (right). (B) Torsional mechanism rendering exploded view. (C) Conceptual overview of experimental protocol. Treadmill belt velocity profiles are across-participant ensemble averages, with shaded regions representing ±1 standard deviation.

over ~340 ms (Golyski et al., 2022)). Perturbations were delivered in either early (onset at ~10% of the gait cycle) or late stance (onset at ~30% of the gait cycle). Within each block, participants experienced 20 perturbations (2 timings x left or right side x 5 repetitions). The perturbations were delivered using an algorithm described in (Golyski et al., 2022), with real-time kinematic heel strike detection being used to estimate the duration of gait cycles from which the desired onset timing of each perturbation was determined. 30–40 steps elapsed between perturbations to allow for a return to steady state walking and to make the perturbations unpredictable (Liu et al., 2018). A conceptual overview of the experiment is shown in Fig. 1C, in addition to perturbation velocity profiles.

2.3. Kinematics and kinetics

82 total retroreflective markers were affixed to each participant (modified human body model 2, (Van Den Bogert et al., 2013)) and the exoskeleton (16 markers were used to track mechanism kinematics), with 5 pelvis and trunk markers attached to the exoskeleton being used to track human body movement. 3D marker trajectories were collected at 100 Hz (Vicon, Oxford, UK). A generic full-body musculoskeletal model ((Rajagopal et al., 2016), 22 rigid bodies, 37 degrees of freedom) was scaled in OpenSim (Delp et al., 2007) for each participant based on a static standing trial where the participant was in the K0 configuration. Models for the various exoskeleton spring conditions were generated by assuming the mass of the exoskeleton was uniformly distributed across the torso segment (i.e., torso mass and inertia were scaled while torso center of mass location was not changed). Exoskeleton torques were estimated using torque–angle relationships determined from benchtop testing (see **Supplementary Material**) together with mechanism kinematics. Joint angles and moments were calculated in OpenSim from unfiltered marker and force data, with outputs being low-pass filtered at 6 and 15 Hz, respectively, using fourth order zero-phase Butterworth filters. Filter properties were similar to those of prior analyses of walking with unilateral belt accelerations (Debelle et al., 2020; Liu et al., 2018). Positions and velocities of all body segments and the whole-body COM were calculated from kinematic data using the OpenSim Body Kinematics tool, as in (Golyski and Sawicki, 2022). Strides were segmented using a 30 N threshold applied to vertical ground reaction forces measured by force platforms embedded within the treadmill. All trials were manually inspected for crossover steps, with 717 of the 880 perturbations being used for all subsequent analyses.

2.4. Whole-body angular momentum

WBAM about the whole-body COM was calculated using a custom Matlab script with inputs of segment masses, inertias, positions, and linear and angular velocities. Segment masses and inertias were obtained from scaled models while positions and velocities were calculated using the OpenSim Body Kinematics tool. These values were used to calculate WBAM according to Eq (1) (Herr and Popovic, 2008; Popovic et al., 2004):

$$\boldsymbol{WBAM} = \sum_{i=1}^{22}\left[\left(\boldsymbol{r}^{i}_{COM} - \boldsymbol{r}_{COM}\right) \times m^{i}\left(\boldsymbol{v}^{i}_{COM} - \boldsymbol{v}_{COM}\right) + \boldsymbol{I}^{i}\boldsymbol{\omega}^{i}\right] \tag{1}$$

where i indicates the segment number (22 total due to the musculoskeletal model), $\boldsymbol{r}_{COM}$ is the position of the whole-body center of mass, $\boldsymbol{r}^i_{COM}$ is the position of the segment's center of mass, m^i is the mass of the segment, $\boldsymbol{v}^i_{COM}$ is the velocity of the segment's center of mass, $\boldsymbol{v}_{COM}$ is the velocity of the whole-body center of mass, $\boldsymbol{I}^i$ is the segment inertia tensor, and $\boldsymbol{\omega}^i$ is the segment angular velocity. WBAM was expressed in the fixed laboratory reference frame and was normalized using the mass of each participant not wearing the exoskeleton, the stature of each participant, and the average walking speed (1.25 m/s).

2.5. Whole-body and joint energetics

Whole-body mechanical power was calculated as described in (Zelik et al., 2015), according to Eq (2):

$$P_{WholeBody} = P_{COM} + P_{per} \tag{2}$$

P_{COM} was the mechanical power of the COM relative to the global frame calculated according to Eq (3), and P_{per} was the mechanical power of the 22 body segments moving relative to the COM according to Eq (4):

$$P_{COM} = \frac{d}{dt}\left(\frac{1}{2}m_{COM}(\boldsymbol{v}_{COM})^2 + m_{COM}\boldsymbol{g}h_{COM}\right) \tag{3}$$

$$P_{per} = \frac{d}{dt}\left(\sum_{i}^{22}\frac{1}{2}\boldsymbol{I}^i\cdot(\boldsymbol{\omega}^i)^2 + \frac{1}{2}m^i\left(\boldsymbol{v}^i_{COM} - \boldsymbol{v}_{COM}\right)^2\right) \tag{4}$$

where in addition to the terms defined in Eq (1), m_{COM} is the mass of the whole body, $\boldsymbol{g}$ is the acceleration due to gravity, and h_{COM} is the vertical position of the whole-body COM. While $P_{WholeBody}$ could also be calculated using ground reaction forces and COM velocities as in (Zelik et al., 2015), kinematic measurements alone were used in this study to avoid the influence of force measurement errors leading to erroneous apparent net gains or losses of system energy during steady locomotion, at the expense of inaccuracies in modelled segment masses and inertias.

Sagittal plane leg joint mechanical powers were calculated as the product of joint moments and their respective joint angular velocities. Joint angular velocities were obtained by differentiating joint angles with respect to time. All kinetic and mechanical energetic measures were normalized to the mass of each participant without the exoskeleton. Mechanical work values were calculated for each stride by integrating the respective mechanical powers with respect to time.

2.6. Statistics

Linear mixed models were used to assess the main effect of exoskeleton stiffness on the principal outcome measures for the pre-perturbation stride ("S-1"), the perturbed stride ("S0"), and the first recovery stride ("S+1"), where strides were defined by the leg ipsilateral to the perturbation. In addition to metrics for exoskeleton characterization, the principal discrete outcome metrics were sagittal WBAM range (H1), whole-body mechanical work (H1), and hip work (H2). These metrics were statistically compared on the S-1 stride to determine steady state effects of the exoskeleton. Differences in these metrics from their steady state values were used to evaluate the S0 and S+1 strides to remove steady state effects of exoskeleton stiffness. The linear mixed models included fixed factors of exoskeleton stiffness, perturbation timing, the interaction of stiffness and timing, and repetition number of the perturbation (i.e., 1–5), in addition to random factors of participant and perturbation side. Bonferroni-corrected pairwise post-hoc tests were calculated from estimated marginal means. Estimated marginal means were also used to calculate 95% confidence intervals (95% CI). All linear mixed models were calculated in SPSS (IBM, Armonk, NY). Lastly, to determine whether the exoskeleton changed the relationship between hip work and whole-body work (H2), we calculated linear regressions between hip work for K0, K1, K2, and K3 conditions and whole-body work in the K0 condition. This was to determine whether the exoskeleton (K1, K2, and K3) resulted in different contributions of the hip to the whole-body work demand during the perturbed stride. Regressions were calculated in Matlab 2024b (MathWorks, Natick, MA). The critical alpha for all statistical tests was set at 0.05.

3. Results

3.1. Exoskeleton mechanics

The exoskeleton produced torque from midstance to toe-off (i.e., 30–66% of the gait cycle; Fig. 2B, F, D, H), with increasing stiffness leading to increasing peak torque during steady state walking ($p<0.001$; 95% CI K1 = [0.042, 0.055], K2 = [0.060, 0.074], K3 = [0.078, 0.092] Nm/kg) and for the perturbed ($p<0.001$; 95% CI K1 = [0.050, 0.062], K2 = [0.075, 0.087], K3 = [0.098, 0.110] Nm/kg) and recovery strides ($p<0.001$; 95% CI K1 = [0.039, 0.054], K2 = [0.055, 0.070], K3 = [0.072, 0.086] Nm/kg; Fig. 2). Peak exoskeleton torques were higher on the perturbed leg during the perturbed stride for early (95% CI [0.087, 0.099] Nm/kg) vs. late stance (95% CI [0.062, 0.074] Nm/kg) perturbations ($p<0.001$). Relative to the perturbed stride, peak exoskeleton torques on the contralateral leg during the recovery stride were lower (95% CI K1 = [0.038, 0.052], K2 = [0.055, 0.069], K3 = [0.071, 0.085] Nm/kg). During steady state walking, higher exoskeleton stiffness also coincided with lower peak mechanism extension angles (Fig. 2A, E, C, G; $p<0.001$; 95% CI K1 = [6.2, 9.2], K2 = [10.3, 13.3], K3 = [12.2, 15.3] degrees of flexion), which persisted through the perturbed stride ($p<0.001$; 95% CI K1 = [4.5, 7.6], K2 = [8.7, 11.8], K3 = [10.8, 14.0] degrees) and the recovery stride ($p<0.001$; 95% CI K1 = [6.6, 9.9], K2 = [10.7, 14.0], K3 = [12.5, 15.8] degrees).

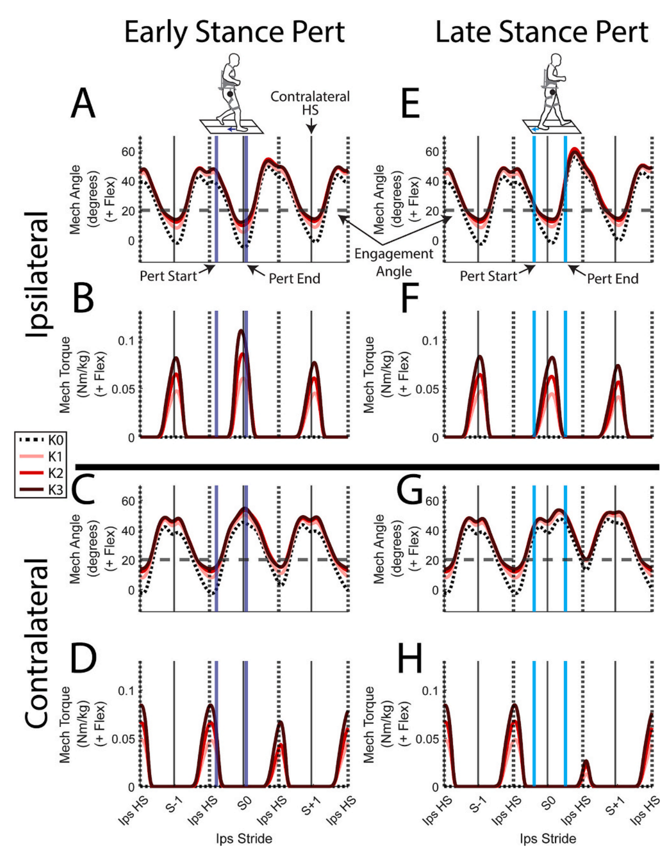

Fig. 2. Across-participant ensemble averaged exoskeleton mechanism angles (A, C, E, G) and torques (B, D, F, H) for the stride before (S-1), stride of (S0), and stride after (S+1) the perturbation. Exoskeleton torques were normalized to the mass of each participant not wearing the device. Standard deviations are omitted for clarity.

3.2. Sagittal whole-body angular momentum

During steady state walking, increasing exoskeleton stiffness resulted in larger sagittal WBAM ranges ($p<0.005$; Fig. 3B, F; 95% CI K0 = [0.034, 0.040], K1 = [0.038, 0.045], K2 = [0.041, 0.047], K3 = [0.042, 0.049]). On the perturbed stride, there was a significant effect of exoskeleton stiffness on the change in WBAM from steady state (Fig. 3C, G; $p=0.029$; 95% CI K0 = [0.021, 0.029], K1 = [0.019, 0.026], K2 = [0.021, 0.028], K3 = [0.022, 0.030]), though the directionality of the relationship relative to the K0 condition was stiffness dependent and no condition resulted in lower WBAM ranges than K0 ($p>0.419$). Pairwise comparisons demonstrated that for the early stance perturbations only, the K3 condition resulted in a larger increase in WBAM range than the K1 condition ($p=0.030$, 95% CI K1 = [0.024, 0.032], K3 = [0.030, 0.038]). On the first recovery stride, there were also significant effects of stiffness (Fig. 3D, H; $p=0.031$; 95% CI K0 = [0.003, 0.008], K1 = [0.003, 0.007], K2 = [0.001, 0.006], K3 = [0.001, 0.006]), though no significant pairwise comparisons ($p>0.494$). With respect to timing of the perturbation, early vs. late stance perturbations resulted in larger increases in WBAM range on the perturbed stride ($p<0.001$; 95% CI early = [0.028, 0.035], late = [0.014, 0.021]), but smaller increases on the first recovery stride ($p<0.001$; 95% CI early = [0.000, 0.005], late = [0.004, 0.008]).

3.3. Whole-body mechanical energetics

There were no significant effects of exoskeleton stiffness on whole-body mechanical work during either timing on any stride ($p>0.226$; Fig. 4). With respect to timing, on the perturbed stride, early vs. late stance perturbations resulted in smaller positive whole-body work demands (Fig. 4C, G; $p<0.001$; 95% CI early = [0.083, 0.156], late = [0.130, 0.202] J/kg). On the first recovery stride, early vs. late stance perturbations resulted in smaller negative whole-body work demands (Fig. 4D, H; $p<0.001$; 95% CI early = [-0.133, -0.062], late = [-0.176, -0.106] J/kg).

3.4. Hip mechanical energetics

During steady state walking, on both sides there was a slight but significant ($p<0.001$) increase in hip work performed with increasing exoskeleton stiffness, driven primarily by differences from the K0 condition (Fig. 5B, F, J, N; 95% CI K0 = [0.183, 0.246], K1 = [0.190, 0.253], K2 = [0.197, 0.260], K3 = [0.198, 0.261] J/kg). On the perturbed stride, there was a significant effect of exoskeleton stiffness on ipsilateral ($p=0.008$; Fig. 5C, E), but not contralateral ($p=0.059$; Fig. 5K, O), hip work from steady state. At the ipsilateral hip, for early stance perturbations, the K2 condition was associated with increased hip work compared to the K1 condition (Fig. 5C; $p=0.048$; 95% CI K1 = [0.136, 0.243], K2 = [0.194, 0.300] J/kg), while for late stance perturbations, the K2 condition was associated with increased hip work compared to the K3 condition (Fig. 5G; $p=0.006$; 95% CI K2 = [0.386, 0.490], K3 = [0.319, 0.423]). On the first recovery stride, there was only an effect of exoskeleton stiffness on the contralateral hip (Fig. 5L, P; $p=0.046$), with decreased hip work in the K1 vs. K0 conditions during the late stance perturbations approaching significance (Fig. 5P; $p=0.051$; 95% CI K0 = [0.062, 0.102], K1 = [0.034, 0.075] J/kg). The effect of timing was significant on both sides and strides ($p<0.001$ for all), with early vs. late stance perturbations resulting in decreased ipsilateral hip work on the perturbed stride (95% CI early = [0.169, 0.263], late = [0.361, 0.455] J/kg) and first recovery strides (95% CI early = [-0.007, 0.029], late = [0.122, 0.157] J/kg). On the contralateral side during the perturbed stride, early vs. late stance perturbations resulted in increased hip work (95% CI early = [0.029, 0.090], late = [-0.240, -0.180] J/kg). On the first recovery stride, early vs. late stance perturbations resulted in decreased ipsilateral and contralateral hip work (95% CI ipsilateral early = [-0.007, 0.029], ipsilateral late = [0.122, 0.157], contralateral early = [-0.024, 0.008], contralateral late = [0.049, 0.081] J/kg). Across-participant ensemble averages of leg joint angles, moments, and knee and ankle powers are included as **supplementary figures** (**Fig. S1-S4**, respectively).

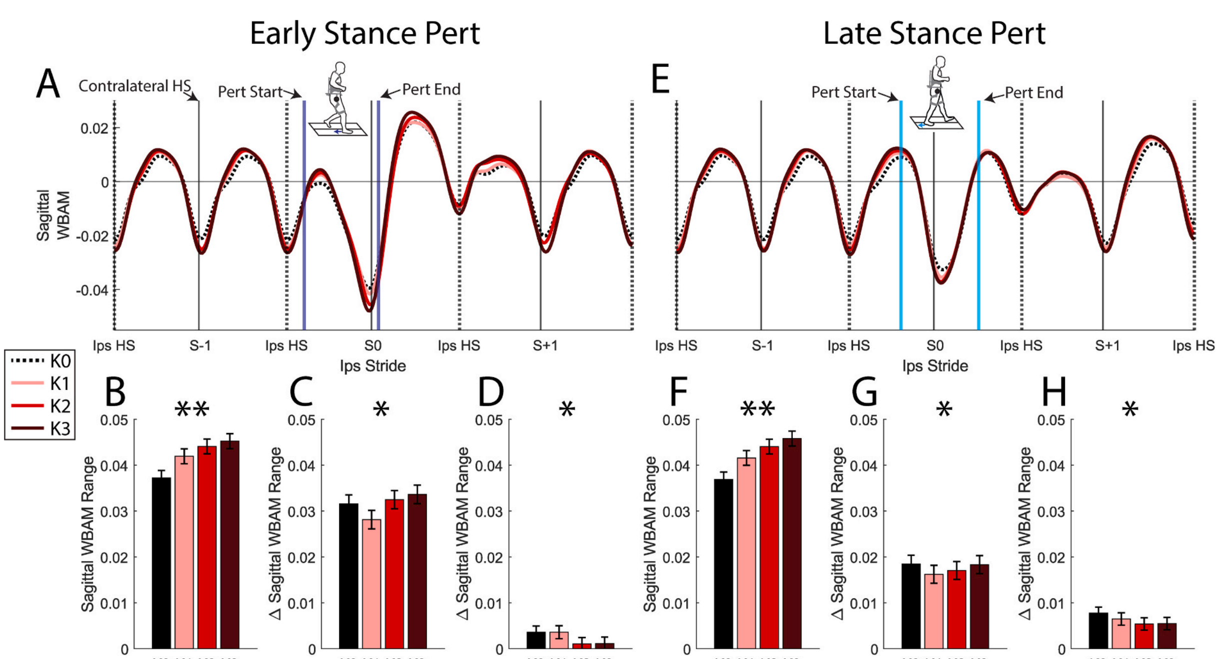

Fig. 3. Exoskeleton effects on stability as measured by sagittal plane whole-body angular momentum (WBAM). Top row: across-participant ensemble averages of sagittal WBAM for the stride before (S-1), during (S0), and after (S+1) the perturbation for early stance perturbations (A) and late stance perturbations (E). Standard deviations are omitted for clarity. Bottom row: sagittal WBAM range during the S-1 stride (B, F), and changes in ranges from steady state levels for the perturbed stride (C, G), and recovery stride (D, H). For all measures, sagittal WBAM was normalized to participant body mass with no exoskeleton, stature, and steady state walking speed (1.25 m/s). Error bars represent ±1 standard error. ** and * represent significant main effects of stiffness with $p<0.001$ and $p<0.050$, respectively. Positive angular momentum is defined as backward pitching.

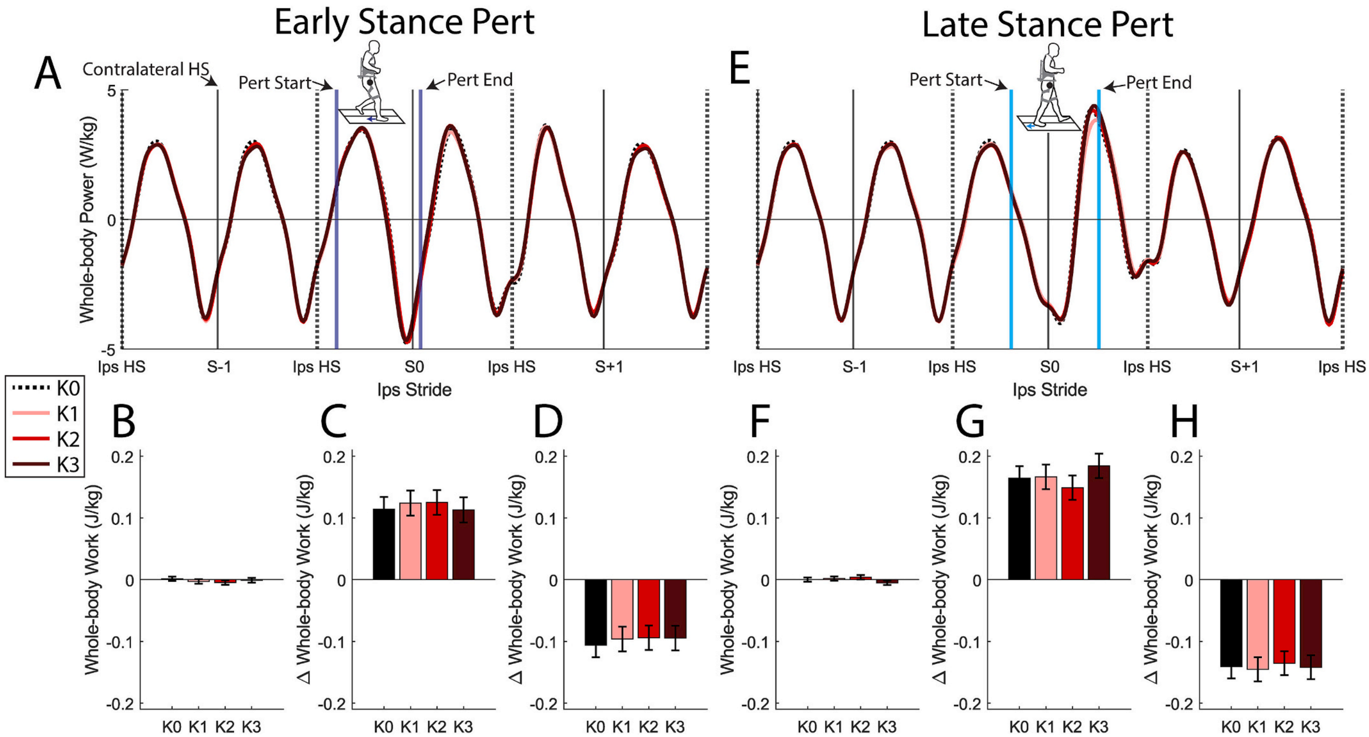

Fig. 4. Exoskeleton effects on whole-body mechanical energetics. Top row: across-participant ensemble averages of whole-body mechanical power for the stride before (S-1), during (S0), and after (S+1) for early stance perturbations (A) and late stance perturbations (E). Standard deviations are omitted for clarity. Bottom row: whole-body mechanical work during the S-1 stride, (B, F), and changes in mechanical work from steady state levels for the perturbed stride (C, G), and recovery stride (D, H). Work and power were normalized to participant body mass with no exoskeleton. Error bars represent ±1 standard error. There were no significant effects of exoskeleton stiffness on any whole-body work value.

3.5. Relating hip work and whole-body work during the perturbed stride

Regressions between whole-body work demands during the perturbed stride and hip work demands during the perturbed stide were only significant for the ipsilateral hip in the K0 and K1 conditions and the contralateral hip in the K1 condition (Fig. 6). Regressions indicated that for each J/kg of whole-body work demand in the K0 condition, the ipsilateral hip contributed 0.94 J/kg in the K0 condition, and 0.82, 0.35, and 0.5 J/kg in the K1, K2, and K3, respectively. Further, for each J/kg of whole-body work demand in the K0 condition, the contralateral hip contributed −0.75 J/kg in the K0 condition, and −0.77, −0.32, and −0.33 J/kg in the K1, K2, and K3 conditions, respectively.

4. Discussion

The main objective of this study was to understand the influence of an elastic hip exoskeleton which resisted hip extension and assisted hip flexion on stability in the anteroposterior direction as quantified by sagittal WBAM range and whole-body mechanical energetics. To accomplish this objective, we imposed destabilizing energetic demands using rapid unilateral anteroposterior belt accelerations while individuals walked with a custom elastic hip exoskeleton. We hypothesized (H1) that an elastic hip exoskeleton would improve stability based on both measures as evidenced by decreased sagittal WBAM range and whole-body mechanical work demands during the perturbed and first recovery strides. We further hypothesized (H2) that the effect of the exoskeleton on mechanical work would be mediated by a shift in hip work in opposition to the whole-body work demand of the perturbation. Since elastic exoskeleton users adapt their kinematics in response to device stiffness, which can lead to non-linear alterations in outcomes as a function of exoskeleton stiffness, we analyzed exoskeleton outcomes across 3 stiffnesses spanning ~0.33–1.0 Nm/deg.

Our first hypothesis (H1) was not supported by our data. For stability quantified by whole-body mechanical work, there was no significant effect of exoskeleton condition on the change in whole-body work during the perturbed stride, which indicates the exoskeleton was not energetically stabilizing. Additionally, for stability quantified by sagittal WBAM range, there were no significant pairwise comparisons relative to the K0 condition, indicating that no spring stiffness was stabilizing relative to walking without a spring when quantified using sagittal WBAM range. However, there was a significant effect of exoskeleton stiffness for perturbations occurring in early stance, with the stiffest exoskeleton condition (K3) being associated with larger changes in sagittal WBAM range from steady state walking than the most compliant exoskeleton condition (K1), indicating diminished stability in the K3 vs. K1 conditions. These findings indicate anteroposterior stability as quantified by sagittal WBAM range and whole-body mechanical work, despite both variables being linked to the angular velocity of body segments and influenced by the perturbation, do not result in consistent conclusions about the stabilizing or destabilizing effects of an intervention.

The significant effect of exoskeleton stiffness on sagittal WBAM range during steady state walking in contrast to the effects of the exoskeleton on the perturbed stride illustrates the importance of using perturbation paradigms to draw conclusions about anteroposterior stability. A larger WBAM range, as usually assessed during steady state walking, has been associated with decreased stability (Hisano et al., 2023; Honda et al., 2019; Silverman and Neptune, 2011), since WBAM is thought to be "tightly regulated" and fluctuate within a narrow range during walking (Herr and Popovic, 2008). Thus, relative to literature, our data suggest the elastic hip exoskeleton was moderately destabilizing during steady state walking, which contrasts with our finding that the exoskeleton had limited effects on stability during perturbed walking. We found mean normalized sagittal WBAM range was 23% higher (from 0.037 to 0.046) in the K0 vs. K3 conditions, which is within the range of previously reported differences in normalized sagittal

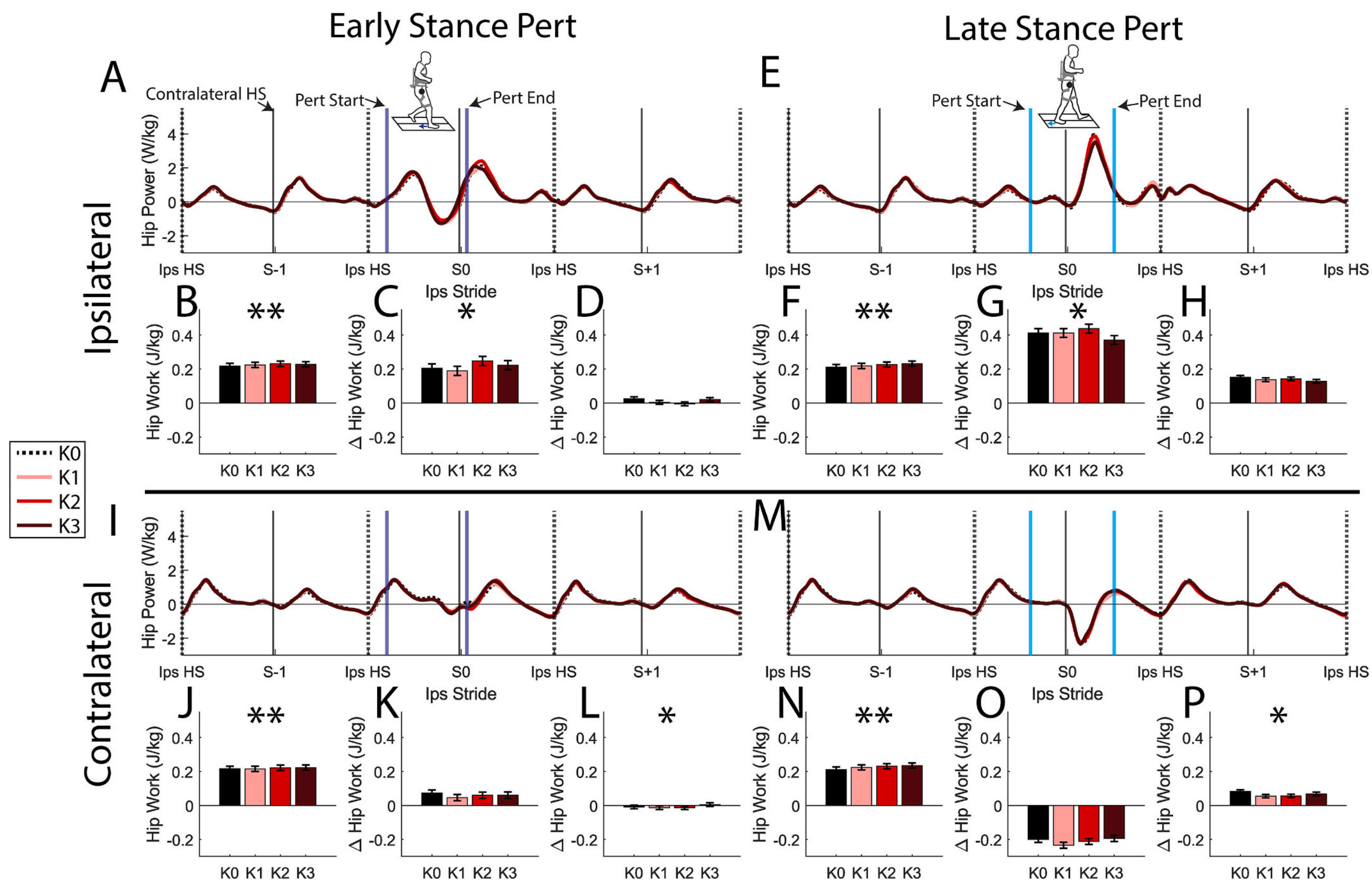

Fig. 5. Exoskeleton effects on the hip ipsilateral to the perturbation for early stance perturbations (A) and late stance perturbations (E), and the hip contralateral to the perturbation for early stance perturbations (I) and late stance perturbations (M). For each side, the top row shows across-participant ensemble averages of sagittal hip mechanical power for the stride before (S-1), during (S0), and after (S+1) the perturbation. Standard deviations are omitted for clarity. Within each side, the bottom row shows sagittal hip mechanical work during the S-1 stride (B, F, J, N), and changes in mechanical work from steady state levels for the perturbed stride (C, G, K, O), and recovery stride (D, H, L, P). Work and power were normalized to participant body mass with no exoskeleton. Error bars represent ±1 standard error. ** and * represent significant main effects of stiffness with $p<0.001$ and $p<0.050$, respectively.

WBAM among individuals with vs. without unilateral transtibial limb loss (45% higher, 0.042 vs. 0.027, respectively) and with vs. without transfemoral limb loss (18.6% higher, 0.076 vs. 0.064, respectively). This effect is unlikely to be caused by differences in exoskeleton mass, as incorporating the added mass of the exoskeleton into WBAM normalization resulted in a 21% increase in WBAM range from the K0 to K3 conditions. Together, these findings suggest future studies should take care when drawing conclusions about stability from WBAM ranges collected during steady state walking. Stability quantified by whole-body mechanical work somewhat avoids this concern since stability cannot be assessed during a "steady state" level ground stride. During steady state level ground walking, there is minimal, and on average across many strides, zero, energy flowing into or out of the body that must be dissipated or re-generated for the body to return to steady state levels. In the context of the perturbation, we found that both early and late stance perturbation timings generally elicited demands of net positive work on the perturbed stride and net negative work on the first recovery stride – demands that were not shifted by the exoskeleton and indicated no effect on "energetic" stability.

Our second hypothesis (H2) was that improved stability as quantified by whole-body work would be mediated by shifts in mechanical work at the hip joints that opposed whole-body energetic demands during the perturbation. This hypothesis was based on previous elastic exoskeletons altering the net work of the joints they target (Collins et al., 2015; Lewis and Ferris, 2011), and shifts in dynamics of plantarflexor muscles to lower forces and altered lengths/velocities during use of elastic ankle exoskeletons (Farris et al., 2013; Nuckols et al., 2020). Comparison of average effects across exoskeleton conditions did not support a connection between local energetic changes induced by the exoskeleton and improvement of stability during the perturbed period. Indeed, the effect of stiffness on mechanical work during the perturbed and first recovery strides at both the whole-body and hip joint levels was minimal. Similar to the conclusions drawn from sagittal WBAM range, we found that although there were significant effects of exoskeleton stiffness during unperturbed walking, these did not carry over into the perturbed stride. However, regressions comparing the whole-body mechanical energetic demand of the perturbations to hip work during the perturbed stride suggested that for higher (i.e., K2 and K3) exoskeleton stiffnesses, our second hypothesis was supported for the ipsilateral hip but rejected for the contralateral hip. We found the ipsilateral hip produced 0.59 and 0.44 J/kg less work per unit of whole-body perturbation work for K2 and K3 stiffnesses vs. the no spring condition, respectively, while the contralateral hip produced 0.43 and 0.42 J/kg more work per J/kg of whole-body perturbation work for K2 and K3 stiffnesses vs. the no spring condition, respectively.

Overall, our results indicated limited effects of the elastic hip exoskeleton on mechanical energetics, but appreciable effects on WBAM – how might this have occurred? One theoretical reason for this is the mathematical attribution of the added mass of the exoskeleton to the trunk segment. However, separating WBAM into contributions of the trunk and the contributions of the legs reveals there was not a vertical shift in trunk angular momentum as would be caused by an increase in inertia or mass, but rather a phase shift (**Fig. S5**). This phase shift of trunk angular momentum together with the invariant fluctuations of the

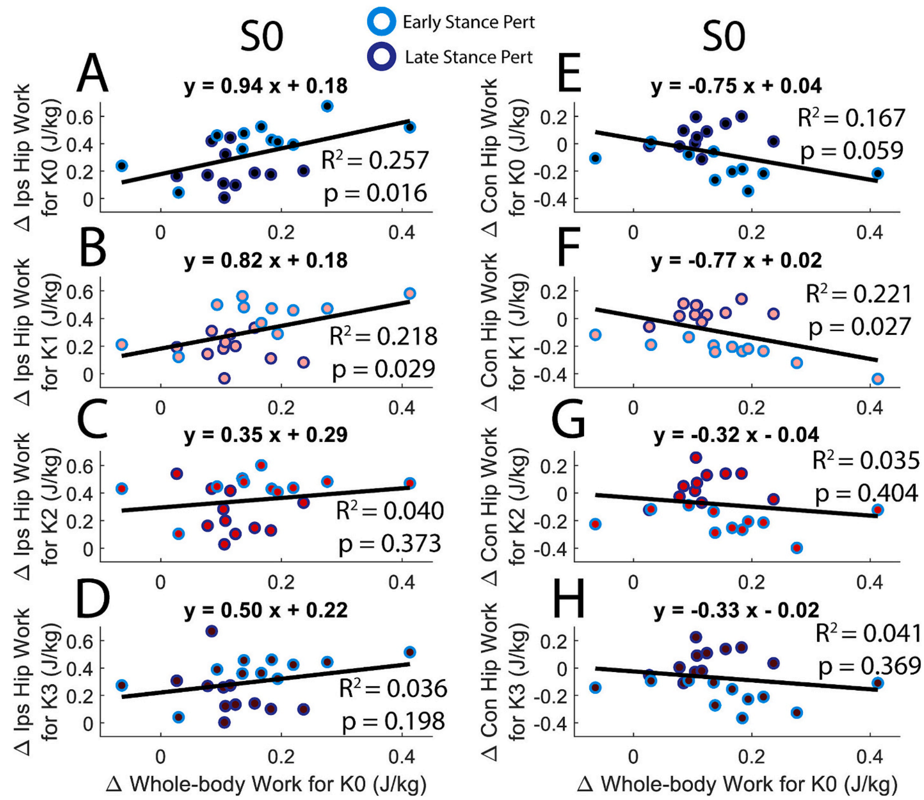

Fig. 6. Regressions investigating the altered the role of the hip in responding to the whole-body work demand on the perturbed stride across exoskeleton conditions. Each point represents the whole-body work demand in the K0 condition vs. the hip work demand for each exoskeleton condition averaged across a given participant and perturbation timing (early and late). A-D = ipsilateral hip work, E-H = contralateral hip work. Work was normalized to participant body mass with no exoskeleton.

leg contribution led to a "constructive interference" which precipitated higher peak to peak fluctuations in WBAM. Thus, the effects of the exoskeleton on anteroposterior stability from the WBAM perspective occurred not from the effects of the exoskeleton on the legs, but instead changes in trunk kinematics induced by the exoskeleton. Additionally, given that trunk dynamics are critical for perturbation recovery (Grabiner et al., 2008), our finding that trunk angular momentum drives WBAM trends also highlights the importance of investigating trunk dynamics in future studies using hip exoskeleton assistance to enhance stability during perturbed walking.

The present study had three important limitations. First, the torque produced by the exoskeleton was lower than anticipated, which likely contributed to the limited effects of the device on stability metrics. Relative to literature, however, our highest stiffness condition produced a peak torque during unperturbed walking of 0.075 Nm/kg, which is 66% larger than the average torque of a low-profile elastic hip flexion device which lowered the metabolic cost of walking in older adults (Panizzolo et al., 2019), and within the range of flexion torques (0.05 to 0.11 Nm/kg) considered to result in changes in joint powers (Haufe et al., 2020). Further, the exoskeleton was designed to produce torques up to 30 Nm (approximately 0.4 Nm/kg) based on unassisted kinematic profiles, and we did not observe large changes in hip angle during device use (**Fig. S1**). Additional analysis of lumbar and mechanism kinematics revealed that this lost device torque was not due to changes in lumbar flexion angle, but rather angular displacements of the mechanism components relative to the body. An accounting of the angular displacements of the individual components of the mechanism indicated that under load there was both a downward pitch of the pelvis section of the mechanism and an upward pitch of the thigh section of the mechanism (**Fig. S6**). Thus, future iterations of this device should adopt more rigid interfaces at both the torso and thigh to improve coupling between body and mechanism kinematics. Future studies seeking to influence stability using an elastic hip exoskeleton should consider emulating an elastic device using a powered exoskeleton (Shafer et al., 2023) to ensure torques are applied independent of exoskeleton fit or using a linear spring in parallel with the quadriceps to consistently provide flexion torque (Haufe et al., 2020; Panizzolo et al., 2019). The second limitation is related to the context of this study. We investigated the effect of the exoskeleton in healthy, able-bodied participants and using stereotyped perturbations. Thus, the effects of the device could be different, and are anticipated to be larger, in balance impaired populations (Honda et al., 2019; Silverman and Neptune, 2011). Further, different types of perturbations could elicit different effects of the device. For example, pelvis pulls (e.g., (Vlutters et al., 2018)) may induce alterations in torso kinematics, which could in turn lead to different device torque profiles compared to treadmill belt accelerations. Lastly, the ability of either stability variable, whole-body work or WBAM, to quantify stability in a clinical context (i.e., fall risk) warrants further study. Larger sagittal WBAM range or mechanical energy fluctuations within a healthy uninjured population may not be representative of increased fall risk, but may instead represent altered motor control strategies to achieve the same level of stability. This limitation can be addressed by evaluating the association between these stability variables and fall frequency or the magnitude of a perturbation required to cause a fall.

To conclude, this study investigated the effects of an elastic hip exoskeleton on anteroposterior stability as quantified by sagittal WBAM range and mechanical energetics during walking with transient unilateral treadmill belt perturbations. While we hypothesized the exoskeleton could improve stability as evidenced by reduced sagittal WBAM range and reduced whole-body mechanical work demand during the perturbed stride, we instead found that no exoskeleton stiffness condition resulted in significantly smaller changes in sagittal WBAM range from steady state levels than the exoskeleton with no spring and that whole-body work demand during the perturbation was not influenced by the exoskeleton. While higher exoskeleton stiffnesses (0.66–1.0 Nm/deg) did result in different contributions of the hip joints to whole-body work during the perturbed stride, changes at both the ipsilateral and contralateral hips offset one another. Our findings also demonstrate: 1) conclusions drawn about anteroposterior stability from sagittal WBAM range do not extend to perturbed walking and 2) changes in trunk dynamics caused by hip flexion assistance may influence sagittal WBAM during walking.

Ethics

All participants provided written informed consent and all protocols were approved by the Institutional Review Board at the Georgia Institute of Technology (Protocol H21076).

Data Accessibility

The biomechanical data for all participants (N = 11) are available at: power.me.gatech.edu/archival-data-from-publications/. Bills of materials and CAD designs for the exoskeleton are available at power.me.gatech.edu/models-2/.

Authors' contributions

Pawel Golyski and Gregory Sawicki conceived of the study and designed the experimental protocol; Pawel Golyski and Nicholas Swaich designed the exoskeleton and carried out the experiments. Pawel Golyski analyzed the data and drafted the manuscript; Pawel Golyski, Nicholas Swaich, Fausto Panizzolo, and Gregory Sawicki edited the manuscript. All authors gave final approval for publication.

CRediT authorship contribution statement

Pawel R. Golyski: Writing – review & editing, Writing – original draft, Visualization, Methodology, Formal analysis, Data curation, Conceptualization. **Nicholas K. Swaich:** Writing – review & editing, Methodology, Investigation, Formal analysis. **Fausto A. Panizzolo:** Writing – review & editing, Formal analysis. **Gregory S. Sawicki:** Writing – review & editing, Supervision, Resources, Project administration, Investigation, Funding acquisition, Formal analysis, Conceptualization.

Funding

This research was supported by the U.S. Army Natick Soldier Research, Development, and Engineering Center (W911QY18C0140 to Gregory Sawicki) and the National Science Foundation (DGE-1650044 to Pawel Golyski).

Declaration of competing interest

The authors declare that they have no known competing financial interests or personal relationships that could have appeared to influence the work reported in this paper.

Acknowledgements

The authors thank Jennifer Leestma for developing the perturbation program. We would also like to thank John Kerr, Harini Mohan, Sparsh Kudrimoti, William Pleasant, Jackson Matray, and Alexis Wilmot for their assistance with data collection. Lastly, we would like to thank David Zink, James de Klerk, and Max Shepherd for their assistance with exoskeleton design.

Appendix A. Supplementary data

Supplementary data to this article can be found online at https://doi.org/10.1016/j.jbiomech.2025.112784.

References

Banala, S.K., Kim, S.H., Agrawal, S.K., Scholz, J.P., 2009. Robot assisted gait training with Active Leg Exoskeleton (ALEX). IEEE Trans. Neural Syst. Rehabil. Eng. 2–8. https://doi.org/10.1109/TNSRE.2008.2008280.

Bennett, B.C., Russell, S.D., Sheth, P., Abel, M.F., 2010. Angular momentum of walking at different speeds. Hum. Mov. Sci. 29, 114–124. https://doi.org/10.1016/j.humov.2009.07.011.

Chen, W., Wu, S., Zhou, T., Xiong, C., 2019. On the biological mechanics and energetics of the hip joint muscle-tendon system assisted by passive hip exoskeleton. Bioinspir. Biomim. 14. https://doi.org/10.1088/1748-3190/aaeefd.

Chiu, V.L., Raitor, M., Collins, S.H., 2021. Design of a Hip Exoskeleton with actuation in frontal and sagittal planes. IEEE Trans Med Robot Bionics 3, 773–782. https://doi.org/10.1109/TMRB.2021.3088521.

Collins, S.H., Bruce Wiggin, M., Sawicki, G.S., 2015. Reducing the energy cost of human walking using an unpowered exoskeleton. Nature 522, 212–215. https://doi.org/10.1038/nature14288.

Debelle, H., Harkness-Armstrong, C., Hadwin, K., Maganaris, C.N., O'Brien, T.D., 2020. Recovery from a forward falling slip: measurement of dynamic stability and strength requirements using a split-belt instrumented treadmill. Front Sports Act Living 2. https://doi.org/10.3389/fspor.2020.00082.

Delp, S.L., Anderson, F.C., Arnold, A.S., Loan, P., Habib, A., John, C.T., Guendelman, E., Thelen, D.G., 2007. OpenSim: open-source software to create and analyze dynamic simulations of movement. I.E.E.E. Trans. Biomed. Eng. 54, 1940–1950. https://doi.org/10.1109/TBME.2007.901024.

Dooley, S., Kim, S., Nussbaum, M.A., Madigan, M.L., 2023. A passive leg-support exoskeleton adversely affects reactive balance after simulated slips and trips on a treadmill. J. Biomech. 151. https://doi.org/10.1016/j.jbiomech.2023.111533.

Farris, D.J., Robertson, B.D., Sawicki, G.S., 2013. Elastic ankle exoskeletons reduce soleus muscle force but not work in human hopping. J. Appl. Physiol. 115, 579–585. https://doi.org/10.1152/japplphysiol.00253.2013.-Inspired.

Golyski, P.R., Sawicki, G.S., 2022. Which lower limb joints compensate for destabilizing energy during walking in humans? J. R. Soc. Interface 19. https://doi.org/10.1098/rsif.2022.0024.

Golyski, P.R., Vazquez, E., Leestma, J.K., Sawicki, G.S., 2022. Onset timing of treadmill belt perturbations influences stability during walking. J. Biomech. 130. https://doi.org/10.1016/j.jbiomech.2021.110800.

Grabiner, M.D., Donovan, S., Bareither, M.L., Marone, J.R., Hamstra-Wright, K., Gatts, S., Troy, K.L., 2008. Trunk kinematics and fall risk of older adults: translating biomechanical results to the clinic. J. Electromyogr. Kinesiol. 18, 197–204. https://doi.org/10.1016/j.jelekin.2007.06.009.

Haufe, F.L., Wolf, P., Riener, R., Grimmer, M., 2020. Biomechanical effects of passive hip springs during walking. J. Biomech. 98. https://doi.org/10.1016/j.jbiomech.2019.109432.

Herr, H., Popovic, M., 2008. Angular momentum in human walking. J. Exp. Biol. 211, 467–481. https://doi.org/10.1242/jeb.008573.

Hisano, G., Murata, H., Kobayashi, T., Major, M.J., Nakashima, M., Hobara, H., 2023. Dynamic balance during walking in transfemoral prosthesis users: step-to-step changes in whole-body and segment angular momenta. IEEE Trans. Neural Syst. Rehabil. Eng. 31, 2893–2902. https://doi.org/10.1109/TNSRE.2023.3290320.

Honda, K., Sekiguchi, Y., Muraki, T., Izumi, S.I., 2019. The differences in sagittal plane whole-body angular momentum during gait between patients with hemiparesis and healthy people. J. Biomech. 86, 204–209. https://doi.org/10.1016/j.jbiomech.2019.02.012.

Lamers, E.P., Zelik, K.E., 2021. Design, modeling, and demonstration of a new dual-mode back-assist exosuit with extension mechanism. Wearable Technol. 2. https://doi.org/10.1017/wtc.2021.1.

Lenzi, T., Carrozza, M.C., Agrawal, S.K., 2013. Powered hip exoskeletons can reduce the user's hip and ankle muscle activations during walking. IEEE Trans. Neural Syst. Rehabil. Eng. 21, 938–948. https://doi.org/10.1109/TNSRE.2013.2248749.

Lewis, C.L., Ferris, D.P., 2011. Invariant hip moment pattern while walking with a robotic hip exoskeleton. J. Biomech. 44, 789–793. https://doi.org/10.1016/j.jbiomech.2011.01.030.

Li, J.M., Molinaro, D.D., King, A.S., Mazumdar, A., Young, A.J., 2021. Design and validation of a cable-driven asymmetric back exosuit. Design and Validation of a Cable-Driven Asymmetric Back Exosuit. https://doi.org/10.1109/TRO.2021.

Liu, C., De Macedo, L., Finley, J.M., 2018. Conservation of reactive stabilization strategies in the presence of step length asymmetries during walking. Front. Hum. Neurosci. 12. https://doi.org/10.3389/fnhum.2018.00251.

Liu, C., Finley, J.M., 2020. Asymmetric gait patterns alter the reactive control of intersegmental coordination patterns in the sagittal plane during walking. PLoS One 15. https://doi.org/10.1371/journal.pone.0224187.

Monaco, V., Tropea, P., Aprigliano, F., Martelli, D., Parri, A., Cortese, M., Molino-Lova, R., Vitiello, N., Micera, S., 2017. An ecologically-controlled exoskeleton can improve balance recovery after slippage. Sci. Rep. 7. https://doi.org/10.1038/srep46721.

Nasiri, R., Ahmadi, A., Ahmadabadi, M.N., 2018. Reducing the energy cost of human running using an unpowered exoskeleton. IEEE Trans. Neural Syst. Rehabil. Eng. 26, 2026–2032. https://doi.org/10.1109/TNSRE.2018.2872889.

Nuckols, R.W., Dick, T.J.M., Beck, O.N., Sawicki, G.S., 2020. Ultrasound imaging links soleus muscle neuromechanics and energetics during human walking with elastic ankle exoskeletons. Sci. Rep. 10. https://doi.org/10.1038/s41598-020-60360-4.

Nuckols, R.W., Takahashi, K.Z., Farris, D.J., Mizrachi, S., Riemer, R., Sawicki, G.S., 2020. Mechanics of walking and running up and downhill: a joint-level perspective to guide design of lower-limb exoskeletons. PLoS One 15. https://doi.org/10.1371/journal.pone.0231996.

Panizzolo, F.A., Bolgiani, C., Di Liddo, L., Annese, E., Marcolin, G., 2019. Reducing the energy cost of walking in older adults using a passive hip flexion device. J. Neuroeng. Rehabil. 16. https://doi.org/10.1186/s12984-019-0599-4.

Patton, J., Brown, D.A., Peshkin, M., Santos-Munné, J.J., Makhlin, A., Lewis, E., Colgate, J.E., Schwandt, D., 2008. KineAssist: design and development of a robotic overground gait and balance therapy device. Top. Stroke Rehabil. 15, 131–139. https://doi.org/10.1310/tsr1502-131.

Pijnappels, M., Bobbert, M.F., Van Dieën, J.H., 2004. Contribution of the support limb in control of angular momentum after tripping. J. Biomech. 37, 1811–1818. https://doi.org/10.1016/j.jbiomech.2004.02.038.

Popovic, M., Hofmann, A., Herr, H., 2004. Angular momentum regulation during human walking: biomechanics and control. In: IEEE International Conference on Robotics and Automation, 2004. Proceedings. ICRA '04. 2004. IEEE, pp. 2405-2411 Vol.3. Doi: 10.1109/ROBOT.2004.1307421.

Rajagopal, A., Dembia, C.L., DeMers, M.S., Delp, D.D., Hicks, J.L., Delp, S.L., 2016. Full-Body musculoskeletal model for muscle-driven simulation of human gait. IEEE Trans Biomed Eng. 63, 2068–2079. https://doi.org/10.1109/TBME.2016.2586891.

Sawicki, G.S., Beck, O.N., Kang, I., Young, A.J., 2020. The exoskeleton expansion: improving walking and running economy. J. Neuroeng. Rehabil. https://doi.org/10.1186/s12984-020-00663-9.

Shafer, B.A., Powell, J.C., Young, A.J., Sawicki, G.S., 2023. Emulator-Based optimization of a Semi-Active Hip exoskeleton concept: sweeping impedance across walking speeds. IEEE Trans Biomed Eng. 70, 271–282. https://doi.org/10.1109/TBME.2022.3188482.

Shamaei, K., Sawicki, G.S., Dollar, A.M., 2013. Estimation of quasi-stiffness of the human hip in the stance phase of walking. PLoS One 8. https://doi.org/10.1371/journal.pone.0081841.

Shepertycky, M., Burton, S., Dickson, A., Liu, Y.-F., Li, Q., 2021. Removing energy with an exoskeleton reduces the metabolic cost of walking. Sci. 1979 (372), 957–960. https://doi.org/10.1126/science.aba9947.

Silverman, A.K., Neptune, R.R., 2011. Differences in whole-body angular momentum between below-knee amputees and non-amputees across walking speeds. J. Biomech. 44, 379–385. https://doi.org/10.1016/j.jbiomech.2010.10.027.

Van Den Bogert, A.J., Geijtenbeek, T., Even-Zohar, O., Steenbrink, F., Hardin, E.C., 2013. A real-time system for biomechanical analysis of human movement and muscle function. Med. Biol. Eng. Compu. 51, 1069–1077. https://doi.org/10.1007/s11517-013-1076-z.

Van Dijk, W., Van Der Kooij, H., 2014. XPED2: a passive exoskeleton with artificial tendons. IEEE Rob. Autom. Mag. 21, 56–61. https://doi.org/10.1109/MRA.2014.2360309.

Vlutters, M., van Asseldonk, E.H.F., van der Kooij, H., 2018. Foot placement modulation diminishes for perturbations near foot contact. Front. Bioeng. Biotechnol. 6, 1–14. https://doi.org/10.3389/fbioe.2018.00048.

Williamson, J.L., Lichtwark, G.A., Sawicki, G.S., Dick, T.J.M., 2023. The influence of elastic ankle exoskeletons on lower limb mechanical energetics during unexpected perturbations. R. Soc. Open Sci. 10. https://doi.org/10.1098/rsos.221133.

Witte, K.A., Fiers, P., Sheets-Singer, A.L., Collins, S.H., 2020. Improving the energy economy of human running with powered and unpowered ankle exoskeleton assistance. Sci. Robot.

Young, A.J., Foss, J., Gannon, H., Ferris, D.P., 2017. Influence of power delivery timing on the energetics and biomechanics of humans wearing a hip exoskeleton. Front. Bioeng. Biotechnol. 5. https://doi.org/10.3389/fbioe.2017.00004.

Zelik, K.E., Takahashi, K.Z., Sawicki, G.S., 2015. Six degree-of-freedom analysis of hip, knee, ankle and foot provides updated understanding of biomechanical work during human walking. J. Exp. Biol. 218, 876–886. https://doi.org/10.1242/jeb.115451.

Zhang, T., Tran, M., Huang, H., 2018. Design and experimental verification of hip exoskeleton with balance capacities for walking assistance. IEEE/ASME Trans. Mechatron. 23, 274–285. https://doi.org/10.1109/TMECH.2018.2790358.